Plasma Physics and Controlled Fusion, Vol. 26, No. 4, pp. 589 to 602, 1984
Printed in Great Britain.

0741-3335/84$3.00 + .00

ION CYCLOTRON RESONANCE HEATING IN THE WISCONSIN LEVITATED OCTUPOLE

C. M. FORTGANG, J. C. SPROTT and E. J. STRAIT
Department of Physics, University of Wisconsin, Madison, WI 53706, U.S.A.

(*Received* 10 *June* 1983)

Abstract—Ion cyclotron resonance heating has been investigated, both experimentally and theoretically, on the Wisconsin Levitated Octupole. Heating of both ions and electrons has been observed. Typically, a two component ion energy distribution is produced (300 and 50 eV) with 500 kW of r.f. power coupled into a 5×10^{12} cm^{-3} plasma. Power is coupled to the plasma with an antenna that also serves as the inductor of an oscillator tank circuit. The oscillator is tunable from 1 to 3 MHz and can be applied for periods up to 10 ms. The experiments were performed with hydrogen, gun-injected plasmas. Most of the theoretical work presented deals with a calculation that predicts the plasma loading. A slab model is used, and the questions of accessibility, polarization and damping of the evanescent radio frequency electromagnetic fields are addressed. It is found that cold plasma theory cannot account for the heating, and therefore hot plasma theory is invoked to explain the results. The loading measurements and theoretical predictions are found to be in reasonable agreement.

1. INTRODUCTION

WAVE heating of magnetically confined plasma has become a major focus of numerous plasma physics experiments and theoretical studies (STIX, 1975; PERKINS, 1977; SCHARER *et al.*, 1977; HOSEA *et al.*, 1979; COLESTOCK *et al.*, 1980; BIDDLE *et al.*, 1981; DAVIS *et al.*, 1983; OWENS *et al.*, 1983).

We report here, high power ICRH experiments on the Wisconsin Levitated Octupole. The experiments were performed with hydrogen, gun-injected plasmas at the fundamental ion cyclotron frequency. This work, in some respects, is an extension of earlier research done on the Small Toroidal Octupole at the University of Wisconsin (BARTER and SPROTT, 1977). The experiments presented here were done on a larger machine, at higher density (10^{12}–10^{13} cm^{-3} vs 10^{10}–10^{11} cm^{-3} in previous experiments), and higher r.f. power ($\sim$500 kW vs $\sim$100 kW in previous experiments). Though similar in design, the new parameter regime brought both some expected and unexpected results. For example, electron drag becomes a power loss channel for the ions, thus making impurity radiation an important process for power balance. Also, the plasma loading is observed to be lighter than was originally expected from a simple density and size scaling from previous experiments.

A theoretical model for calculating the loading is presented, and with certain simplifying assumptions the questions of accessibility, polarization, and damping are addressed. The model provides a predicted effective plasma resistance which can be compared with experimental measurement. Measurements of the evanescent toroidal component of the r.f. electric field in the presence of plasma can be made and provide an additional test of the theory.

Atomic processes dominate the power balance, the most important being charge exchange for the ions, and impurity radiation for the electrons.

2. APPARATUS AND DIAGNOSTICS

The Wisconsin Levitated Octupole has been described by FORSEN *et al.* (1970). The machine is a toroidal device with four internal rings which are inductively driven to

form an octupole poloidal field. A capacitor bank and the primary windings on an iron core form an LC resonant circuit with a half-period of 43 ms. Plasma experiments are run near peak field, at ~21 ms. The rings are supported by prods which can be pneumatically removed for 20 ms during which the plasma experiment is performed. A combination of magnetic pressure and inertia keeps the rings stationary or levitated until the prods are reinserted after the experiment. Most of the data presented here were without levitation. The maximum available poloidal field is 11.6 kG at the inner rings and 5.6 kG at the outer rings. The poloidal field strength is specified by the capacitor bank charging voltage (maximum 5 kV). The center of the machine has three closely spaced field nulls, and so most of the plasma is situated in a minimum average B magnetic well.

Ion temperatures are measured with a charge exchange analyser and an electrostatic gridded energy analyser probe. The charge exchange diagnostic is a single channel, 127°, curved plate, electrostatic analyser with a nitrogen stripping cell. It is located on the top lid of the machine azimuthally away from the antenna. We measure typically a two component, Maxwellian, ion distribution function as shown in Fig. 1. The relative populations indicated in Fig. 1 are obtained assuming that the two components of the ion energy distribution undergo charge exchange with neutral hydrogen of the same density. Electron temperatures are measured with Langmuir probes, and the plasma density is measured with a 70 GHz microwave interferometer.

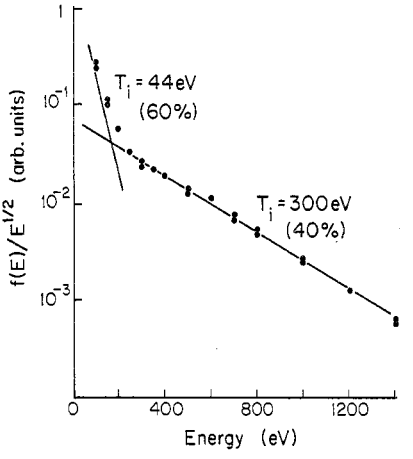

FIG. 1.—Typical two-component ion energy distribution as measured with a charge exchange analyser.

The r.f. source (Fig. 2) is a tuned-plate, tuned-grid, class C, push-pull oscillator. The tubes are operated with tuned-grid feedback, and the oscillation frequency (1–3 MHz), is chosen by adjusting the capacitance of the plate tank circuit. The antenna is Faraday shielded, spans 120° in the toroidal direction, and serves as the inductor of the plate tank circuit. The source can supply ~2 MW of r.f. power to the tank circuit for 10 ms. Typically 500 kW is coupled to a 5.0×10^{12} cm^{-3} plasma. The plasma loading is determined by measuring by what amount the plasma spoils the Q of the tank circuit. The ratio of circulating current (I_c), measured by a calibrated pick-up loop located under the antenna, to the d.c. drive current (I^-) coming from

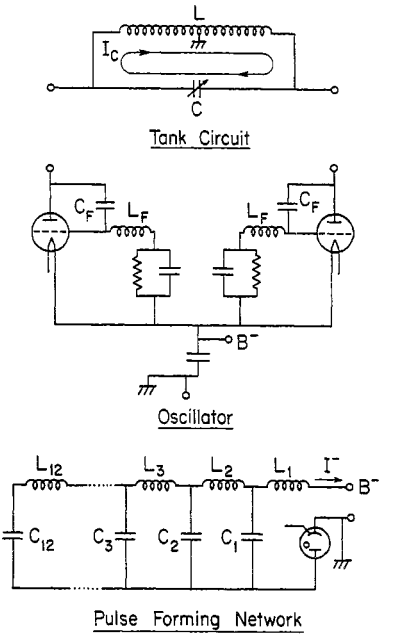

FIG. 2.—Three major components of the r.f. heating system. The center-tapped tank circuit inductor also serves as the antenna.

the pulse forming network, provides an indication of the Q. Since the oscillator is operated class C, the fundamental r.f. drive current I_d is not easily measured and so the Q cannot be directly determined from the simple relation $Q = I_c/I_d$. However, using known resistive loads, and thus a known Q, the calibration is determined in terms of the easily measured quantities I_c and I^-. The Q without plasma is measured and determines the effective series resistance without plasma (96 mΩ). The total power dissipated in the circuit is $\omega L I_c^2/Q$, and the antenna losses are subtracted to get the power dissipated in the plasma, P_{plasma}. We define the plasma radiation resistance as $R_{\text{RAD}} = P_{\text{plasma}}/I_c^2$. Typically we observe coupling efficiencies of $\sim 50\%$, that is, about equal amounts of power are dissipated in the plasma and in the antenna and shields.

Figure 3 shows the Octupole poloidal field lines, the position of the antenna, Faraday shield, and a typical, resonant, mod-B surface. There are two classifications of flux surfaces: private flux, which encircles one ring, and common flux, which encircles all four rings. The separatrix, ψ_{sep}, is the flux surface that separates the two regions of flux. Note that there are actually 3 separatrices, each passing through one of the 3 field nulls. The usual single field null for an octupole is non-degenerate in this case due to the machine wall noses which allow for the levitation. The outermost dashed line in Fig. 3 is called the critical surface, ψ_{crit}, and marks the boundary between average good and average bad curvature. As a matter of convenience, the poloidal flux surfaces are labelled in units of Dories with 10 Dories being the total flux that enters the machine through the gap. At the time of peak field (21 ms) $\psi_{\text{sep}} \simeq 5.7$, $\psi_{\text{crit}} \simeq 7.8$ and in the lower outer bridge $\psi \simeq 2.5$ is at the ring. At maximum field strength, 10 Dories corresponds to 0.72 Webers of poloidal flux.

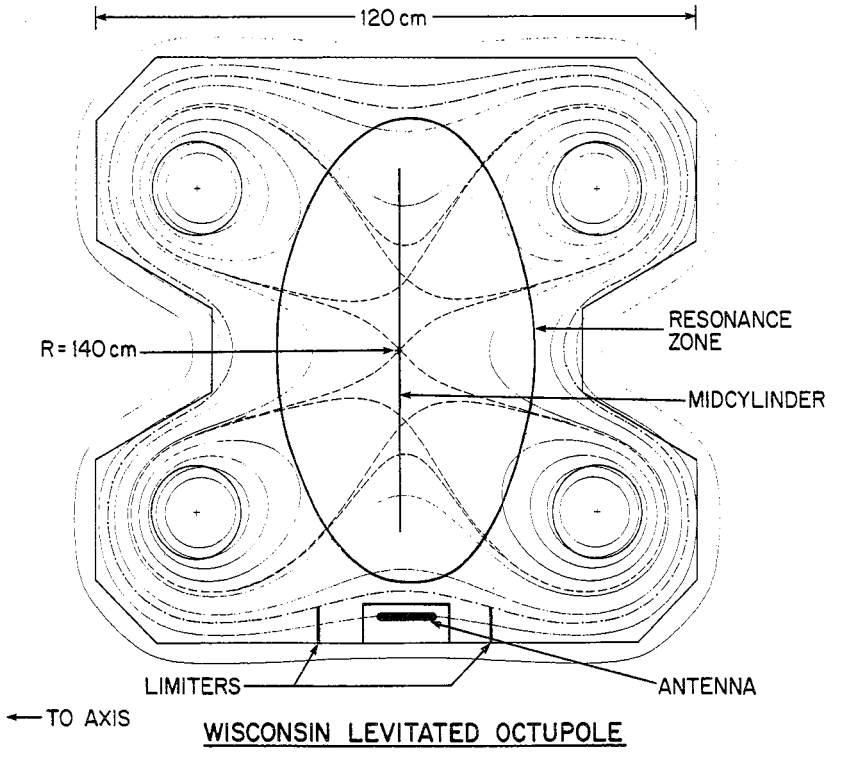

FIG. 3.—Octupole poloidal field lines with a typical resonance zone. The antenna is Faraday shielded, spans 120° in the toroidal direction, and is located on the mid-cylinder.

3. HEATING THEORY

Fundamental heating of ions requires the presence of a left-hand, circularly-polarized component of the r.f. electric field at a region in the plasma where the local ion gyrofrequency matches the frequency of the r.f. The theoretical approach evolves in a systematic manner from the usual homogeneous cold plasma theory to the hot plasma corrections and finally to a damping model from which the plasma loading can be predicted. We start by considering cold plasma theory as formulated by STIX (1962). We use the standard slab coordinate system to model the plasma in the region near the antenna. The magnetic field lines lie in the z-direction (major radius), any gradients lie in the x-direction (vertical), and everything is assumed symmetric in the y-direction (toroidal). Assuming $|E_z| \ll |E_x|$ and $|E_z| \ll |E_y|$ as done by STIX (1975), the polarization in the ion cyclotron range of frequencies from the cold plasma wave equation is

$$P = \frac{iE_x}{E_y} = \frac{\omega}{\omega_c} \frac{1}{\left(1 + \frac{k_z^2 c^2}{\omega_p^2}\left(1 - \frac{\omega_c^2}{\omega^2}\right)\right)}$$

where $P = +1$ for the right circular polarization, -1 for left circular polarization and 0 or $\pm\infty$ for linear polarization, ω is the r.f. frequency, ω_c the ion gyrofrequency,

ω_p the ion plasma frequency, and k_z the parallel wavenumber. The important point is that for $\omega = \omega_c$, $P = 1$, and the electric field is right circularly polarized for all values of density and parallel wavenumber. Since the heating of ions depends on the presence of a left circularly polarized component of the r.f. electric field at the resonance zone, the cold plasma model would predict zero heating. Digressing from the question of polarization for the moment we predict the magnitude of the r.f. electric field at the resonance zone using an inhomogeneous cold plasma slab model. The cold plasma wave equations become (BERS *et al.*, 1980)

$$\frac{\partial^2 E_y}{\partial y^2} + \frac{(Sk_0^2 - k_z^2)^2 - D^2 k_0^4}{Sk_0^2 - k_z^2} E_y = 0$$

$$E_x = \frac{iDk_0^2}{Sk_0^2 - k_0^2}$$

where S and D have the usual cold plasma definitions as defined by STIX (1962) and k_0 is the vacuum wavenumber. The differential equation for E_y is solved numerically using density and magnetic field profiles typical of the experiment near the antenna. The numerical results show no singularity in E_y at the point where $Sk_0^2 = k_z^2$. A detailed discussion of this apparent singularity has been given by STIX (1960). The equation is also solved for the vacuum case. The results show that the y-component of the r.f. electric field is evanescent and that the evanescent length with plasma is only $\sim 15\%$ shorter than the vacuum case in the region up to, and slightly beyond, the resonance zone. The E_y component of the r.f. electric field is measured with a magnetic loop both in vacuum and in the presence of plasma. The probe used to measure E_y is not

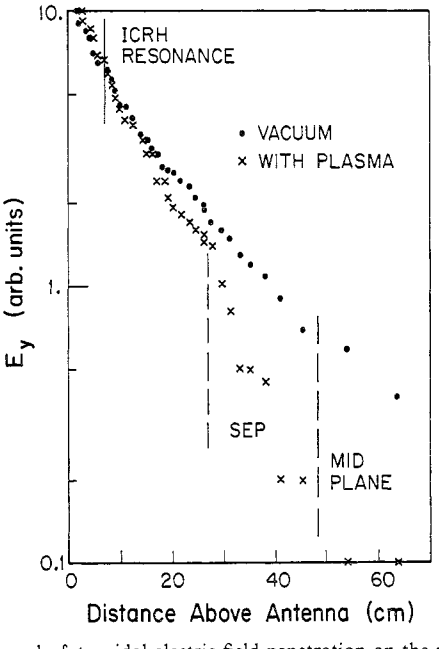

FIG. 4.—Measured r.f. toroidal electric field penetration on the mid-cylinder.

the usual local magnetic pickup loop which with $k_y = 0$ measures dE_y/dx or B_z. The magnetic probe used here is long (in x) and narrow (in y) and effectively integrates the curl E equation by measuring all the flux (B_z) between the probe tip and the wall. With $k_y = 0$, and one end of the probe outside the machine (where $\mathbf{E} = 0$), $\int \mathbf{E} \cdot d\mathbf{l}$ around the loop has a contribution from the tip only and so the signal is proportional to E_y at the end of the probe. The results of the measurements are shown in Fig. 4. The plasma depresses the r.f. electric field near the $B = 0$ axis, but the fields penetrate well up to the ion cyclotron resonance zone indicating good qualitative agreement with the cold plasma theory. However, the cold plasma theory still predicts the electric field to be purely right circularly polarized at the resonance zone. If the width of the zone of elliptical polarization between the antenna (linear polarization) and the resonance zone (circular polarization) were negligible ($\lesssim$ ion gyroradius) then we might argue that it is a good approximation to use the vacuum field polarization (linear) despite the fact that cold plasma theory predicts the fields to be purely right circularly polarized exactly at the position of the resonance. However, for the densities and temperatures in the present experiment, the width of this zone, as determined from solving for $E_y(x)$ and $E_x(x)$, is not negligible, and so hot plasma theory is invoked to account for the heating.

To lowest order the hot plasma corrections (McVEY, 1978) to the cold plasma conductivity tensor elements, S and D are,

$$S = k_0^2 + \frac{1}{2}\sum_\alpha \varepsilon_\alpha \mu_1 \qquad D = \frac{1}{2}\sum_\alpha \varepsilon_\alpha \nu_1$$

where

$$\varepsilon_\alpha = \frac{\omega_p \alpha^2 k_0^2}{\omega k_z v_a}$$

$$\mu_1 = Z_1(\xi_1) + Z_{-1}(\xi_1)$$

$$\nu_1 = Z_1(\xi_1) - Z_{-1}(\xi_{-1})$$

$$\xi_1 = \frac{\omega^+ \omega_{c\alpha}}{k_z v_\alpha}.$$

Here α indicates the particle species, v_α is the thermal speed $= (2kT_\alpha/m_\alpha)^{1/2}$ and Z is the plasma dispersion function of argument ξ. This lowest order correction essentially takes into account a broadening of the resonance zone due to a Doppler shifted r.f. frequency as seen by the ions as they move along field lines. The Doppler shift is larger for short wavelength modes.

The vacuum E_y field is measured to have an approximate gaussian profile off the mid-cylinder at a constant height above the antenna,

$$E_y = E_{y0} e^{-(z/\gamma)^2}$$

where γ is the gaussian width and depends on the height (y) above the antenna. The vacuum field is Fourier analysed, and the plasma response to the polarization is calculated for each k_z component and then inverse Fourier transformed numerically

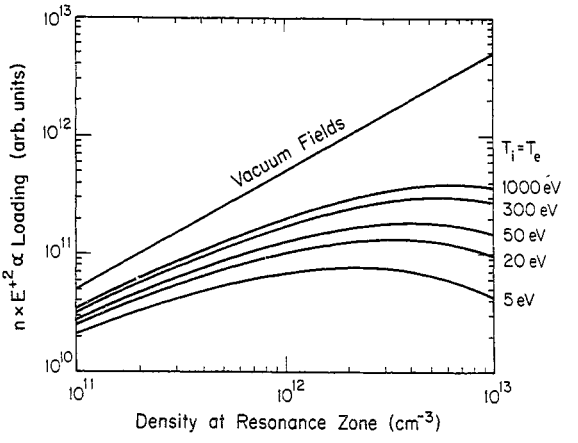

FIG. 5.—Theoretical loading dependence on plasma temperature for a given k_z spectrum.

to get the magnitude of E^+ at the resonance zone (FORTGANG, 1983). It is found for example, for a 1×10^{13} cm^{-3} plasma density at the resonance zone, and $T_i = T_e = 300$ eV, and a k_z spectrum determined by setting $\gamma = 8.6$ cm, that $|E^+/E^-| = 0.23$. The temperature dependence of the loading as determined by this heating theory is shown in Fig. 5. We plot the product nE^{+2}, which is proportional to the loading, as a function of density for various plasma temperatures. The k_z spectrum for this case was determined by setting $\gamma = 8.6$ cm and is equivalent to what is measured experimentally near the antenna. Note that as the density drops the plasma shielding of E^+ becomes less severe as expected. For our experiments, the plasma density where the resonance zone comes closest to the antenna is usually in the range of $1.0–4.0 \times 10^{12}$ cm^{-3}. For these densities and lower, the loading as predicted by this model is not very sensitive to the plasma temperature above 20 eV.

The heating rate is determined by introducing an imaginary part to the r.f. drive frequency ($\nu \ll \omega$) and then calculating the power absorbed by the plasma per unit volume according to the relation

$$\frac{dP}{dV} = (\sigma \cdot \mathbf{E}) \cdot \mathbf{E}$$

where σ is the cold plasma conductivity tensor modified with a dissipative mechanism introduced through the effective collision frequency ν. This model was used by BARTER and SPROTT (1977) to calculate the heating rate in the Small Toroidal Octupole, and their result in a slightly different form is

$$P = \pi e \int n |E^+|^2 \, \delta(B - B_0) dV$$

where B_0 is the magnetic field at the ion cyclotron resonance, P is the power absorbed, and e is the electronic charge. The magnitude of E^+ at the resonance zone is estimated from the hot plasma slab model and depends on the plasma temperature and density as well as the k_z spectrum set up by the antenna and introduced through the parameter γ. Note that though the expression for the power absorbed is the same as that used

by BARTER and SPROTT (1977) here we include the plasma effects on E^+ whereas in the earlier work the vacuum electric field was used. The results of the heating theory are presented along with the experimental measurements in the next section.

4. LOADING AND HEATING RESULTS

Figure 6 shows how the loading varies with magnetic field strength, expressed in terms of the charging voltage on the poloidal field capacitor bank. The data were taken at a reduced r.f. power level of 125 kW. The loading was normalized to the separatrix density (9.3×10^{12} cm$^{-3} \pm 10\%$) for the different field settings. The top theoretical curve shows the damping model with the vacuum electric field (assuming the plasma had no effect on the magnitude or polarization of the r.f. electric field). The second theoretical curve takes into account the hot plasma effects for a value of $\gamma = 8.6$ cm. As mentioned above, gamma is the parameter in the hot plasma theory that determines the k_z spectrum. Since the ion temperature is observed to vary somewhat linearly with magnetic field (discussed below) this effect was put into the theoretical curve by having T_i vary from 75 eV at $B_p = 3.5$ kV to 150 eV at $B_p = 5.0$ kV. T_e was set to 40 eV for all fields. It turns out, however, because the plasma shielding has a weak temperature dependence, that putting in a field-dependent ion temperature has only a small effect on the theoretical curve. The loading is nearly independent of magnetic field because, as the magnetic field strength is lowered and the resonance zone moves closer to the antenna, the r.f. electric field strength increases but the density at the resonance zone decreases. Since the loading is proportional to nE^{+2}, these effects tend to cancel. The hot plasma theoretical curve decreases at higher fields because the resonance zone is in a region of higher density and thus the plasma shielding of E^+ is more effective (Fig. 5). However, the experimental data do not show the same qualitative feature that the loading is less at the higher fields. One possible explanation is that at the higher field settings the resonance zone is in a region of greater magnetic field line curvature which means a greater departure from the slab model approximation. Whereas in the slab approximation, energy must propagate

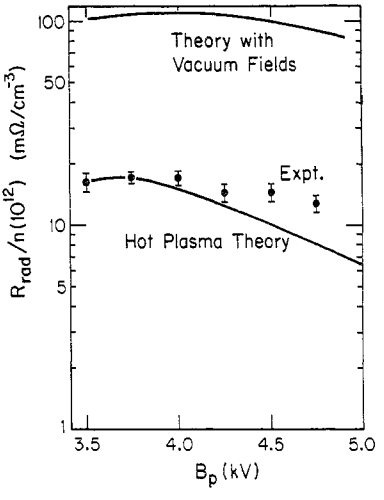

FIG. 6.—Loading dependence on poloidal magnetic field. Magnetic field is expressed in volts on the capacitor bank.

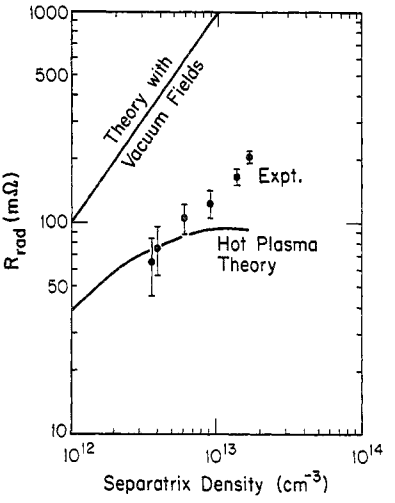

FIG. 7.—Loading dependence on density. Loading at higher densities is heavier than predicted by a hot plasma slab model.

across field lines directly from the antenna to the resonance zone, in the Octupole, energy can be transmitted to the resonance zone near the center of the machine along field lines that curve down past the sides of the antenna. This effect is not treated in the slab model.

Figure 7 shows how the loading scales with density for a constant magnetic field strength at 4.5 kV on the poloidal magnetic field capacitor bank which corresponds to a field of 1.12 kG at the Faraday shield. Again we include the theoretical result using the r.f. vacuum electric field. It is interesting to note that the experimental data scale less than linearly with density, more like $n^{0.7}$. This is in qualitative agreement with the observation that the plasma shielding of E^+ is more complete as the density increases. The theoretical curve with the hot plasma correction is for $\gamma = 8.6$ cm, $T_i = 150$ eV, and $T_e = 40$ eV. The theoretical plot shows the loading begin to saturate at the higher densities (for reasons already discussed) whereas the experimental data continue to rise. Other coupling mechanisms besides ion cyclotron damping, such as excitation of electrostatic ion cyclotron waves near the perpendicular ion cyclotron resonance and/or fast waves, may become important at the higher densities.

The r.f. target plasmas are produced with a coaxial Marshall gun (MARSHALL, 1960). A typical shot is shown in Fig. 8. The r.f. is turned on simultaneously with gun injection and turned off 9.5 ms into the shot. The ion temperatures in Fig. 8 were measured with a charge exchange analyser. By 2 ms into the shot a hot tail appears which for this case (4.5 kV on the B_p bank) is at 300 eV. It has been observed that the electron temperature is very sensitive to machine cleanliness. The shot shown in Fig. 8 is for a clean machine. For a dirty machine the electron temperature falls for the first few milliseconds due to the high impurity concentration and then recovers as the low Z impurities start to burn out.

The r.f. does effect both the particle confinement and reflux rate. Figure 9 shows the interferometer signal for various charging voltages on the pulse forming network (PFN). The voltage on the PFN is proportional to the antenna voltage or the square root of the r.f. power. In Fig. 9 the highest r.f. power case and the case with gun

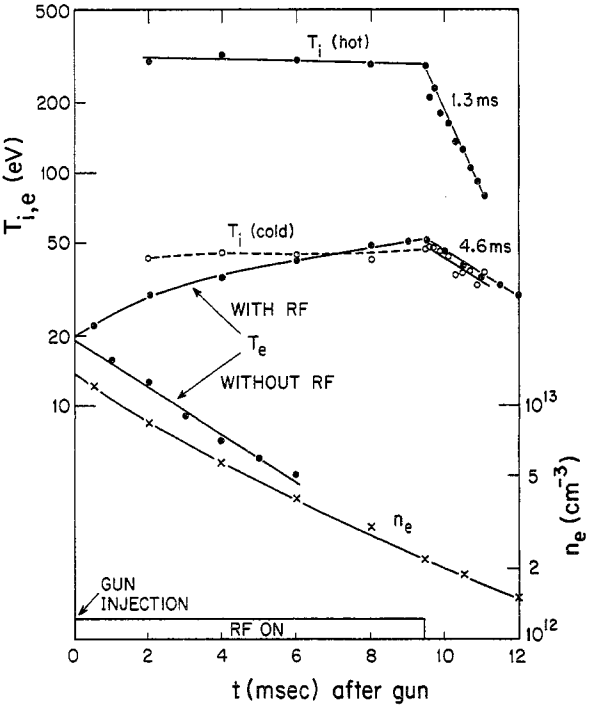

FIG. 8.—Typical shot. Ion temperature is measured with a charge exchange analyser, electron temperature with a Langmuir probe, and density with a microwave interferometer.

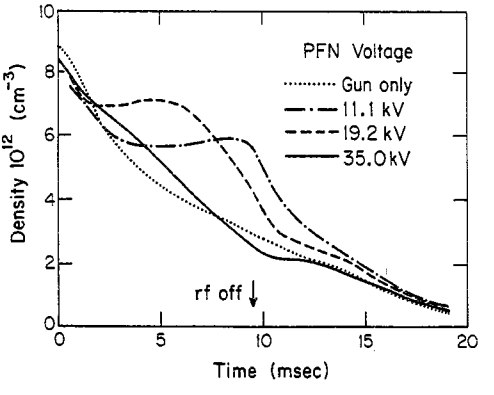

FIG. 9.—Interferometer signal showing decay of plasma density for various r.f. power levels.

only have similar density traces. However, at intermediate power levels the density is higher than without r.f., indicating enhanced reflux. Apparently there are two competing processes. Plasma particle confinement is worse with r.f., but at the low power levels the enhanced reflux gives rise to a net increase in density. As the power is raised, plasma is lost at a rate fast enough to cancel the incoming cold hydrogen gas and impurities.

The hot ion temperature is strongly dependent on magnetic field strength as illustrated in Fig. 10. The abscissa is the magnetic field at the antenna. It is interesting

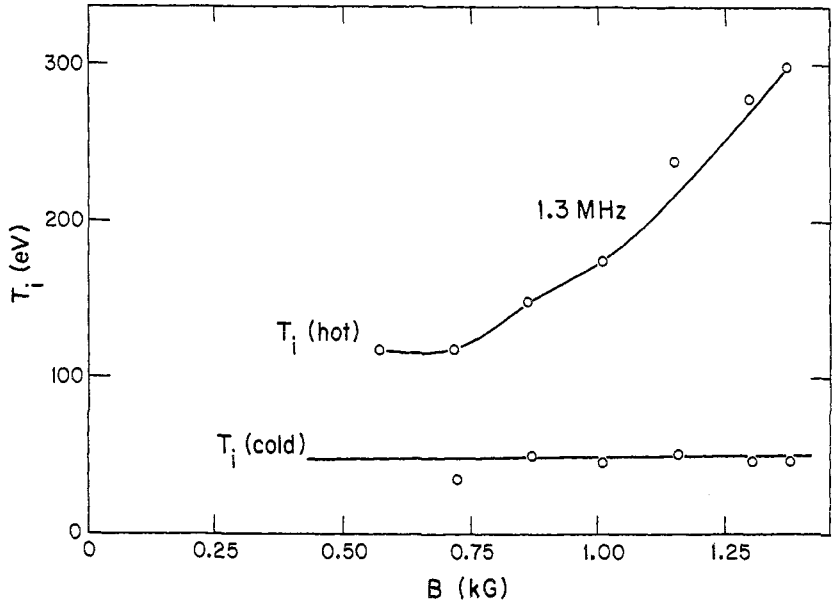

FIG. 10.—Hot ion temperature rises with poloidal magnetic field strength. Magnetic field is expressed in kG at the antenna.

to compare these data with Fig. 6 which shows that the loading is only weakly dependent on the magnetic field. Therefore, the ion temperature dependence on magnetic field must be related to confinement rather than heating. One possibility for the hot ion temperature dependence on magnetic field is that the higher fields have the resonance zone farther from the machine wall where the neutral density is lower, yielding a lower charge exchange rate. However, it has been observed that the hot ion temperature, as opposed to the magnitude of the hot ion population, is fairly insensitive to changes in gettering and thus hydrogen reflux rate. Other possibilities are truncation of the ion energy distribution function at high energies (>2 keV) due to a gyroradius limit in the region where the resonance zone crosses the mid-cylinder near the antenna, and anomalous B-dependent radial transport. It is not well understood at this time why the hot ion temperature is dependent on magnetic field whereas the loading is not. A gridded ion energy analyser probe was used to investigate ion temperature profiles. Profiles were taken in the bridge region azimuthally away from the antenna. Therefore, ions heated over the antenna drift toroidally and move along field lines poloidally in order to reach the probe. Ion temperature and ion saturation current profiles near the end of the r.f. pulse are shown in Fig. 11. The probe can be oriented in two directions with respect to the magnetic field to read either the "perpendicular" or "parallel" ion temperature. The saturation current peaks on the separatix ($\psi = 5.75$), as it usually does in non-r.f.-heated plasmas, but the ion temperature peaks in the common flux region at $\psi \simeq 6.5$ which is the flux surface that crosses the resonance zone near the antenna. (The flux surface that is tangent to the bottom of the resonant mod-B surface for this case is $\psi = 6.8$.) An electron temperature profile taken on the mid-cylinder, directly above the antenna, shows similar behavior with T_e peaking between $\psi = 6.5$ and 6.8.

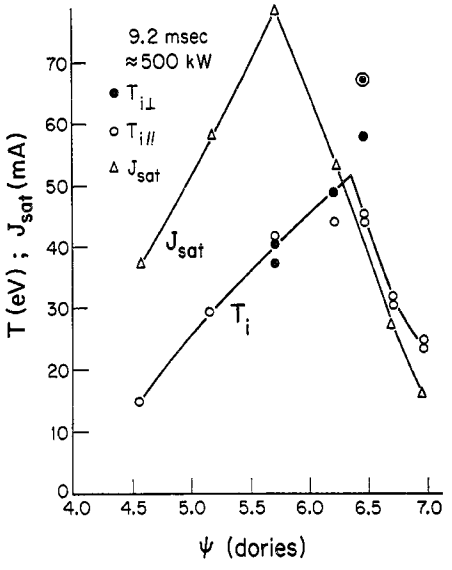

FIG. 11.—Profiles in the bridge region. Ion temperature is obtained with a gridded ion energy analyser probe.

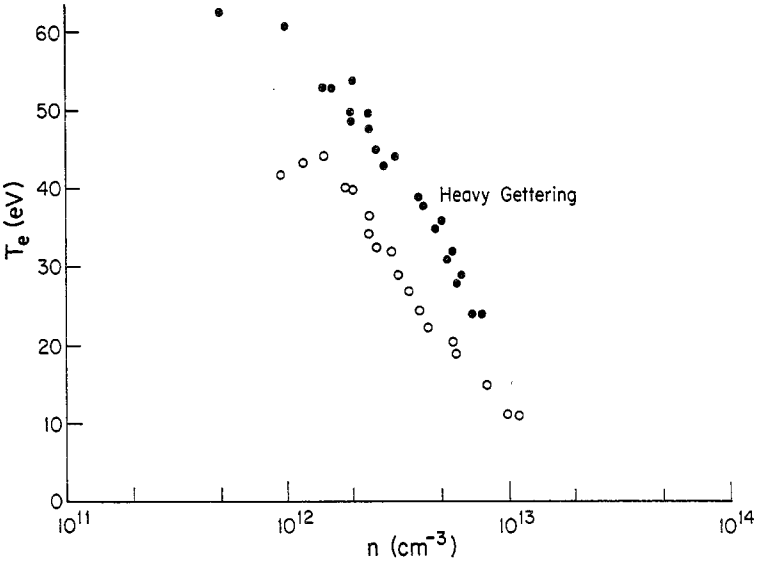

FIG. 12.—Electron temperature is sensitive to machine wall conditions.

The electron temperature is observed to be very sensitive to machine wall conditions. Figure 12 shows that 30–40% increases in T_e are made by turning up the titanium getters. It has been observed that one signature of a clean machine is T_e rising monotonically in time during a shot. A dirty machine, even at full r.f. power, will have T_e fall from the initial 15–20 eV during the first few milliseconds of the r.f. pulse before starting to rise.

With highly convoluted field lines and an antenna that spans 120° toroidally, the Octupole is a truly three-dimensional machine. This fact makes it difficult to model all the atomic and classical particle effects that are taking place. However, global type measurements with a bolometer and the charge exchange analyser indicate that impurity radiation and charge exchange are the dominant energy loss mechanisms. Calculations considering only classical ion heat conduction predict very large and sharply peaked ion temperature profiles that are not consistent with the experimental data. Electron energy confinement times have been measured anywhere from ~ 1 to ~ 5 ms depending on machine cleanliness. The measured hot ion temperature varies little with electron energy confinement, consistent with the assertion that charge exchange is dominant for the hot ion species in a mid-10^{12} cm^{-3} plasma. As a check to determine if coulomb collisions between the various species (hot ions, cold ions and electrons) is consistent with the observed temperatures, a simple zero-dimensional computer code was written to calculate the time evolution of the temperature for each species. The processes included are: coulomb collisions between the various species, charge exchange on the ions (using a neutral density of 1×10^{10} cm^{-3} which is a factor of 3–5 above the machine base pressure between shots), a loss term for the electrons to represent impurity radiation, and r.f. power into the hot ions. The calculated equilibration times for the species are all within the range of 1.0–2.5 ms, and experimental parameters are used wherever possible (e.g. input r.f. power, plasma density, initial temperature, fraction of hot ion). The results of this simple model are within a factor of two of the experimentally measured temperatures and temperature decay times.

5. SUMMARY

Ion and electron heating have been observed with the application of radio frequency power in the ion cyclotron range of frequencies. Electron and ion temperatures are raised to 40–60 eV with an ion tail at 300 eV, which otherwise, without the application of r.f., would be near 10 eV or less.

The toroidal electric field penetrates to the ion cyclotron resonance zone in accordance with an inhomogeneous cold plasma slab model. The heating theory is tested by comparing the plasma loading with a theoretical heating rate calculation including warm plasma effects. The theory and experiment are in reasonable agreement.

Acknowledgements—The assistance of J. BARTER, T. LOVELL and J. LAUFENBERG with the design and construction of the r.f. source is appreciated. We also thank R. DEXTER and S. PRAGER for helpful discussions and G. SEVERN for assistance with data acquisition. This work was supported by the U.S. Department of Energy.

REFERENCES

BARTER J. D. and SPROTT J. C. (1977) *Plasma Physics* **19**, 945.

BERS A., JACQUINOT J. and LISTER G. (1980) *Heating in Toroidal Plasmas, Proc. 2nd Joint Grenoble–Varenna Int. Symp.* Vol. I **569**, CEC, Brussels.

BIDDLE A. P. and SPROTT J. C. (1981) *Plasma Physics* **23**, 679.

COLESTOCK P. L., DAVIS S. L., HOSEA J. C., HWANG D. Q. and THOMPSON H. R. (1980) *Heating in Toroidal Plasmas, Proc. 2nd Joint Grenoble–Varenna Int. Symp.* Vol. I **471**, CEC, Brussels.

DAVIS S. L., PDX and PLT GROUPS (1983) *Plasma Physics* **25**, 189.

FORSEN H. K., KERST D. W., BREUN R. A., CAVALLO A. J., DRAKE J. R. and SPROTT J. C. (1970) *Fourth European Conference on Controlled Fusion and Plasma Physics* **24**, CNEN, Rome.

FORTGANG C. M. (1983) Ph.D. Thesis, University of Wisconsin.

HOSEA J. C., BERNABEI S., COLESTOCK P. L., DAVIS S. L., EFTHIMION P., GOLDSTON R. J., HWANG D. Q., MEDLEY S. S., MUELLER D., STRACHAN J. and THOMPSON H. (1979) *Phys. Rev. Lett.* **43**, 1802.

MARSHALL J. (1960) *Physics Fluids* **3**, 134.
MCVEY B. D. (1978) Ph.D. Thesis, University of Wisconsin.
OWENS T. L., MULLEN J. H., BAITY F. W., DAVIS W. A., ELDRIDGE O. C. and HILLIS D. L. (1983) *Nucl. Fusion* **23**, 49.
PERKINS F. W. (1977) *Nucl. Fusion* **17**, 1197.
SCHARER J. E., MCVEY B. D. and MAU T. K. (1977) *Nucl. Fusion* **17**, 297.
STIX T. H. (1960) *Physics Fluids* **3**, 19.
STIX T. H. (1962) *Theory of Plasma Waves*, McGraw Hill, New York.
STIX T. H. (1975) *Nucl. Fusion* **15**, 737.